Pharmacokinetic Modeling of (R)-[11C]verapamil to Measure the P-Glycoprotein Function in Nonhuman Primates

Garcia Varela, Lara; Vállez García, David; Kakiuchi, T; Ohba, Hiroyuki; Nishiyama, S; Tago, T; Elsinga, Philip H.; Tsukada, Hideo; Colabufo, Nicola Antonio; Dierckx, Rudi

Published in:
Molecular pharmaceutics

DOI:
10.1021/acs.molpharmaceut.0c01014

molecular pharmaceutics

pubs.acs.org/molecularpharmaceutics

Article

Pharmacokinetic Modeling of (*R*)-[^{11}C]verapamil to Measure the P-Glycoprotein Function in Nonhuman Primates

Lara García-Varela, David Vállez García, Takeharu Kakiuchi, Hiroyuki Ohba, Shingo Nishiyama, Tetsuro Tago, Philip H. Elsinga, Hideo Tsukada, Nicola A. Colabufo, Rudi A.J.O. Dierckx, Aren van Waarde, Jun Toyohara, Ronald Boellaard, and Gert Luurtsema*

Cite This: https://dx.doi.org/10.1021/acs.molpharmaceut.0c01014

Read Online

ACCESS | Metrics & More | Article Recommendations | Supporting Information

ABSTRACT: (*R*)-[^{11}C]verapamil is a radiotracer widely used for the evaluation of the P-glycoprotein (P-gp) function at the blood–brain barrier (BBB). Several studies have evaluated the pharmacokinetics of (*R*)-[^{11}C]verapamil in rats and humans under different conditions. However, to the best of our knowledge, the pharmacokinetics of (*R*)-[^{11}C]verapamil have not yet been evaluated in nonhuman primates. Our study aims to establish (*R*)-[^{11}C]verapamil as a reference P-gp tracer for comparison of a newly developed P-gp positron emission tomography (PET) tracer in a species close to humans. Therefore, the study assesses the kinetics of (*R*)-[^{11}C]verapamil and evaluates the effect of scan duration and P-gp inhibition on estimated pharmacokinetic parameters. Three nonhuman primates underwent two dynamic 91 min PET scans with arterial blood sampling, one at baseline and another after inhibition of the P-gp function. The (*R*)-[^{11}C]verapamil data were analyzed using 1-tissue compartment model (1-TCM) and 2-tissue compartment model fits using plasma-corrected for polar radio-metabolites or non-corrected for radio-metabolites as an input function and with various scan durations (10, 20, 30, 60, and 91 min). The preferred model was chosen according to the Akaike information criterion and the standard errors (SE %) of the estimated parameters. 1-TCM was selected as the model of choice to analyze the (*R*)-[^{11}C]verapamil data at baseline and after inhibition and for all scan durations tested. The volume of distribution (V_T) and the efflux constant k_2 estimations were affected by the evaluated scan durations, whereas the influx constant K_1 estimations remained relatively constant. After P-gp inhibition (tariquidar, 8 mg/kg), in a 91 min scan duration, the whole-brain V_T increased significantly up to 208% ($p < 0.001$) and K_1 up to 159% ($p < 0.001$) compared with baseline scans. The k_2 values decreased significantly after P-gp inhibition in all the scan durations except for the 91 min scans. This study suggests the use of K_1, calculated with 1-TCM and using short PET scans (10 to 30 min), as a suitable parameter to measure the P-gp function at the BBB of nonhuman primates.

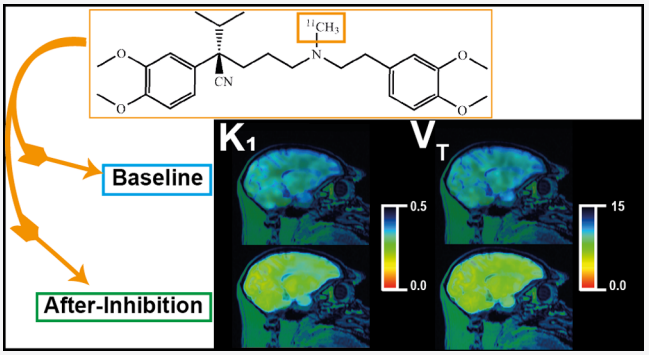

KEYWORDS: *ABC transporters, brain imaging, efflux transporters, kinetics, P-gp tracers, rhesus monkeys*

1. INTRODUCTION

(*R*)-[^{11}C]verapamil is a radiotracer used to assess the P-glycoprotein (P-gp) function at the blood–brain barrier (BBB). Verapamil is a calcium channel blocker that is used in the treatment of cardiovascular diseases such as hypertension and arrhythmias,[1] and it is also characterized as a substrate for the efflux transporter P-gp. Therefore, [^{11}C]-verapamil has been used to assess the P-gp function in the human brain by positron emission tomography (PET).[2,3]

P-gp is a transmembrane protein that belongs to the ATP binding cassette transporter family. This transporter uses the energy provided by hydrolysis of ATP to move endogenous and exogenous compounds across the membranes.[4] The P-gp transporter at the BBB is expressed at the luminal side of the endothelial cells, where it pumps a wide variety of substances from the brain to the blood, protecting the central nervous system (CNS) from harmful damage.[5] P-gp dysfunctions have been related to the onset and progression of several neurodegenerative diseases and psychiatric disorders.[6−8] Furthermore, numerous unrelated CNS drugs are P-gp substrates and, therefore, dysfunction in the P-gp transporter can alter the concentration of these drugs in the brain, causing toxicity issues or decreases in drug efficacy.[9,10] Thus, it is of interest to evaluate the P-gp function *in vivo* with PET imaging,

Received: October 13, 2020
Revised: December 2, 2020
Accepted: December 2, 2020

which is a noninvasive technique and an excellent tool for quantification of biological processes.[11−13] The P-gp function was evaluated for the first time in 1996 using a racemic mixture of [^{11}C]verapamil,[2] and since then, the P-gp function has been extensively studied in humans with this tracer.[7,8,14−20]

[^{11}C]verapamil was first prepared and evaluated as a racemic mixture.[2] However, the (*R*) and (*S*)-verapamil enantiomers showed differences in the rate of metabolism, affinity to calcium channels, plasma protein binding, and clearance that complicate the pharmacokinetic quantification of the racemic tracer.[14,21] Therefore, one of the enantiomers had to be selected for labeling. As (*R*)-[^{11}C]verapamil showed less radiometabolites and lower affinity to calcium channels than (*S*)-[^{11}C]verapamil, it was selected as the most adequate tracer for measuring the P-gp function.[21]

Since then, several studies have reported the ability of (*R*)-[^{11}C]verapamil to measure the P-gp function.[13] For instance, after the administration of a P-gp inhibitor, the P-gp function is decreased and, consequently, the radiotracer is accumulated inside the brain.[22−24] This tracer has a very high affinity for the P-gp transporter and, therefore, at baseline conditions, when the P-gp transporter is working adequately, the tracer uptake is very low because the P-gp transporter pumps most of the tracer out of the brain.[11,25] Novel PET tracers with lower P-gp affinity have been developed to achieve higher tracer uptake in the brain at baseline conditions.[10,11]

The development of new P-gp tracers that have lower affinity to the P-gp transporter (weak P-gp tracers)[26,27] requires kinetic comparison with (*R*)-[^{11}C]verapamil, which is considered as the reference P-gp PET tracer because its kinetics have been widely evaluated in rats and humans under different conditions.[16,28−30] This comparison may lead to a greater understanding of the kinetic properties of weak and avid substrates. Weak P-gp tracers, such as [^{11}C]-metoclopramide and [^{18}F]MC225, have been evaluated in rats and also in nonhuman primates that are more closely related to humans biologically.[26,27,31] However, to perform a head-to-head comparison in nonhuman primates, a kinetic modeling evaluation of (*R*)-[^{11}C]verapamil needs to be performed in monkeys first. So far, only the kinetics of racemic [^{11}C]verapamil were evaluated.[32−34] One study has assessed the kinetics of (*R*)-[^{11}C]verapamil in rhesus monkeys, but it did not provide a full kinetic evaluation of the tracer.[35]

This study aims to assess the kinetics of (*R*)-[^{11}C]verapamil tracer at baseline and after the inhibition of the P-gp function using different scan durations (10, 20, 30, 60, and 91 min) and exploring different compartmental models. Moreover, the paper aims to determine the most suitable and reliable parameter to measure the P-gp function (and its change) at the BBB of nonhuman primates.

2. EXPERIMENTAL SECTION

2.1. Chemicals and Synthesis of the Tracer. Tariquidar (MedChemExpress, New Jersey, USA) was used as a P-gp inhibitor.[24,29,36] Tariquidar solution for intravenous injection was prepared as previously described,[37] with 11 mg of tariquidar methanesulfonate hydrate suspended in 3 mL of saline solution, and the injection volume was adjusted to the weight of each monkey (8 mg/kg of body weight). Radiosynthesis and quality control of (*R*)-[^{11}C]verapamil were performed as described previously.[21]

2.2. Animals. Three healthy male rhesus monkeys (*Macaca mulatta*; Hamri Co. Ltd., Ibaraki, Japan) were included in this study that was performed at the Central Research Laboratory, Hamamatsu Photonics (Hamamatsu, Japan), in collaboration with the Tokyo Metropolitan Institute of Gerontology (Tokyo, Japan). The animals were housed individually in a controlled environment (24 ± 4 °C, 50 ± 20% of humidity under a 14 h light/10 h dark cycle) and maintained and handled in strict accordance with the recommendations of the National Institute of Health and the guidelines of the Ethics Committee of the Central Research Laboratory, Hamamatsu Photonics (approval HPK-2016-07A), and the Institutional Animal Care and Use Committee of Tokyo Metropolitan Institute of Gerontology (approval 16067).

2.3. Data Collection. *2.3.1. Experimental Design.* Each nonhuman primate underwent two PET scans with (*R*)-[^{11}C]verapamil. One was performed at baseline conditions and the second one after the inhibition of the P-gp function with tariquidar. The time interval between the scans was 2 h, except for one animal where it was 2 months due to technical issues. Tariquidar was slowly injected through a catheter inserted into a saphenous vein 15 min before the PET scans at a dose of 8 mg/kg of body weight. Table 1 shows the body weight of the monkeys on the scanning day, the day of the scan, and the hour of radiotracer injection.

Table 1. Design of the Experiments

		(*R*)-[^{11}C]verapamil		
nonhuman primates	scan	experiment date dd/mm/yyyy	hour of injection (hour:min)	body weight (kg)
subject 1	baseline	27/12/2016	10:59	8.2
subject 1	after inhibition	27/12/2016	14:45	8.2
subject 2	baseline	17/02/2017	11:01	6.1
subject 2	after inhibition	17/02/2017	14:03	6.1
subject 3	baseline	28/02/2017	12:45	7.2
subject 3	after inhibition	26/12/2016	14:01	6.6

2.3.2. PET Imaging Acquisition and Reconstruction. The same acquisition protocol was used in a previous study.[37] Briefly, 1 week before the first PET scan, a brain T_1-weighted magnetic resonance imaging (MRI) scan of the animal was made (Signa Excite HDTx 3.0T, GE Healthcare).[38] Brain PET scans were acquired using a high-resolution animal PET scanner (SHR-38000, Hamamatsu Photonics). All nonhuman primates underwent dynamic PET scans with arterial blood sampling. Monkeys were anesthetized (2.5% sevoflurane) during the arterial cannulation and their transport, but they were awake during the scans and the head was immobilized using a fixation device. The animals were positioned in the camera in a sitting position with stereotactic coordinates aligned paralleled to the orbitomeatal plane.

Prior to tracer injection, a rotating ^{68}Ge/^{68}Ga rod source was used to perform the transmission scan (60 min), and its information was used for attenuation correction of the PET images. Next, animals were injected with (*R*)-[^{11}C]verapamil (more information in Table 2) at the start of the emission scan (91 min) *via* the saphenous vein over a period of 30 s as a single bolus.

PET images were reconstructed using the filtered back projection method with a Hanning filter of 4.5 mm in SHR-38000 Reconstruction software (Hamamatsu Photonics) and were composed of 49 frames (6 × 10, 6 × 30, 12 × 60, and 25 × 180 s).

https://dx.doi.org/10.1021/acs.molpharmaceut.0c01014
Mol. Pharmaceutics XXXX, XXX, XXX−XXX

Table 2. Subject Information and Properties of (*R*)-[^{11}C]verapamil

		(*R*)-[^{11}C]verapamil			
nonhuman primates	scan	body weight (kg)	injected dose (MBq)	molar activity (GBq/μmol)	injected mass (nmol)
subject 1	baseline	8.2	893.6	118.2	7.6
subject 1	after inhibition	8.2	919.3	80.6	11.4
subject 2	baseline	6.1	968.8	20.5	47.4
subject 2	after inhibition	6.1	981.8	49.5	19.8
subject 3	baseline	7.2	1020.2	55.5	18.4
subject 3	after inhibition	6.6	941.1	85.3	11.0

2.3.3. Arterial Blood Sampling. As has been described before,[37] after the administration of the tracer, 19 blood samples (0.5 mL) were drawn from a cannula placed in the posterior tibial artery at selected time points (8, 16, 24, 32, 40, 48, 56, and 64 s and 1.5, 2.5, 4, 6, 10, 20, 30, 45, 60, 75, and 90 min). Then, the plasma and blood were separated by centrifugation (12,000 rpm, 60 s), and the radioactivity was measured using a gamma counter (1480 Wizard, PerkinElmer). The total amount of blood removed from the animal was less than 35 mL/day in each animal.

2.3.4. Metabolite Analysis. Parent fraction and polar radioactive metabolites of (*R*)-[^{11}C]verapamil in arterial blood samples were determined following the tracer injection (16, 40, and 64 s and 6, 10, 30, 45, 60, 75, and 90 min). A 0.2 mL volume of ethanol was added to the 0.1 mL of plasma fraction to deproteinize the samples. After centrifugation (13,400 rpm,12,100*g*, for 90 s), the samples were analyzed using thin-layer chromatography plates (silica gel 60 F254, Merk) with a mobile phase of ethyl acetate/trimethylamine (9/1). The parent (Rf = 0.55) and polar-metabolized (Rf = 0.0, origin) fractions were assessed using a phosphor imaging plate and a bioimaging analyzer (FLA-7000, Fuji Film).

The percentage of the polar radio-metabolites in plasma was calculated for each animal by fitting a single exponential equation to the values obtained from the metabolite analysis, using an iterative nonlinear least-squares approach (GraphPad Prism version 7.02, California, USA): $Y = Y_0 \times \exp(-K_e \times X)$,[39] where Y is the percentage of the parent tracer at different time points, Y_0 is the intercept, K_e is the first-order elimination constant, and X is the time.

2.4. Analysis of PET Data. *2.4.1. Time−Activity Curves of Blood Sampling: Input Function.* Time−activity curves (TACs) were determined using the activity of the whole blood and plasma and expressed as a standardized uptake value (SUV): SUV = radioactive concentration/(injected dose/body weight). The radioactivity measured in blood samples was corrected for decay from the time point of tracer administration. The plasma SUV−TAC corrected for polar radio-metabolites (*i.e.*, metabolite-corrected plasma) was calculated by multiplying the SUV values of plasma samples by the percentage of parent tracer.

A single exponential equation was fitted to the radio-metabolite-corrected SUV−TAC individually using the values after the peak (from 360 to 5400 s) by an iterative nonlinear least-squares approach (GraphPad Prism version 7.02, California, USA): $Y = Y_0 \times \exp(-K_e \times X)$, where Y represents the SUV values at different time points, Y_0 is the intercept, K_e is the first-order elimination constant, and X is the time. This approach allows the determination of the rate of tracer elimination (K_e) and the biological half-life ($T_{1/2}$): $T_{1/2} = \ln(2)/K_e$.[40]

2.4.2. PET/MRI Analysis. Images were processed using PMOD v3.8 software (PMOD Technologies, Zürich, Switzerland). All the scans were registered to a reference MRI template[41−43] as previously described[37] and the following volumes of interest (VOI) were selected for further analysis: basal ganglia, brainstem, cerebellum, cingulate cortex, orbitofrontal cortex, hippocampus, hypothalamus, insular cortex, midbrain, occipital cortex, parietal cortex, striatum, temporal cortex, thalamus, white matter, and a VOI covering the whole brain. This registration procedure and region analysis have been previously described.[37]

The registration of the images was performed as follows. First, the MRI of the animal was registered to the reference MRI using a 3 probability maps normalization.[44] Then, (*R*)-[^{11}C]verapamil PET images were aligned to their corresponding MRI by rigid transformation using a summation of all frames. For baseline scans, the (*R*)-[^{11}C]verapamil after-inhibition PET images were used as a reference because of the difficulties in the registration of MRI with the baseline PET images (the latter showing lack of anatomical information in the image and limited brain radiotracer uptake).

2.4.3. Pharmacokinetic Analysis. Several models were fitted to the VOI TACs, with the plasma-corrected for polar radio-metabolites (metabolite-corrected plasma) or non-corrected plasma TACs and the whole-blood TACs as the input function. The pharmacokinetic modeling was performed using PMOD v3.8 software.

First of all, the input functions from each animal were corrected for blood delay. The blood delay was calculated using the whole-brain TAC, and then this value was fixed for the rest of the regions. The compartmental models evaluated were the 1-tissue compartment model (1-TCM), the 2-tissue compartmental model (2-TCM), and the irreversible 2-TCM. All the models were assessed using either a fixed fractional blood volume (vB) (3, 4, 5, 6, or 7%) or using vB as a fit parameter. Data sets with different scan durations (10, 20, 30, 60, and 91 min) were analyzed in order to explore its effect on the model preference and the parameter's estimates. The compartmental model analyses were performed twice, once with the plasma-corrected for polar radio-metabolites and then with the plasma non-corrected for radio-metabolites as the input function. No boundary restrictions were applied for the fit of the parameters during the kinetic analysis.

Akaike information criterion (AIC) was used to choose the most optimal kinetic model for each scan duration and type of scan (baseline or after inhibition). The standard errors (SE %) of the estimated parameters were also taken into consideration during model selection.

Several common kinetic parameters, that is, the influx constant K_1, the volume of distribution (V_T), and the efflux constant k_2, were compared between baseline and after-

https://dx.doi.org/10.1021/acs.molpharmaceut.0c01014
Mol. Pharmaceutics XXXX, XXX, XXX−XXX

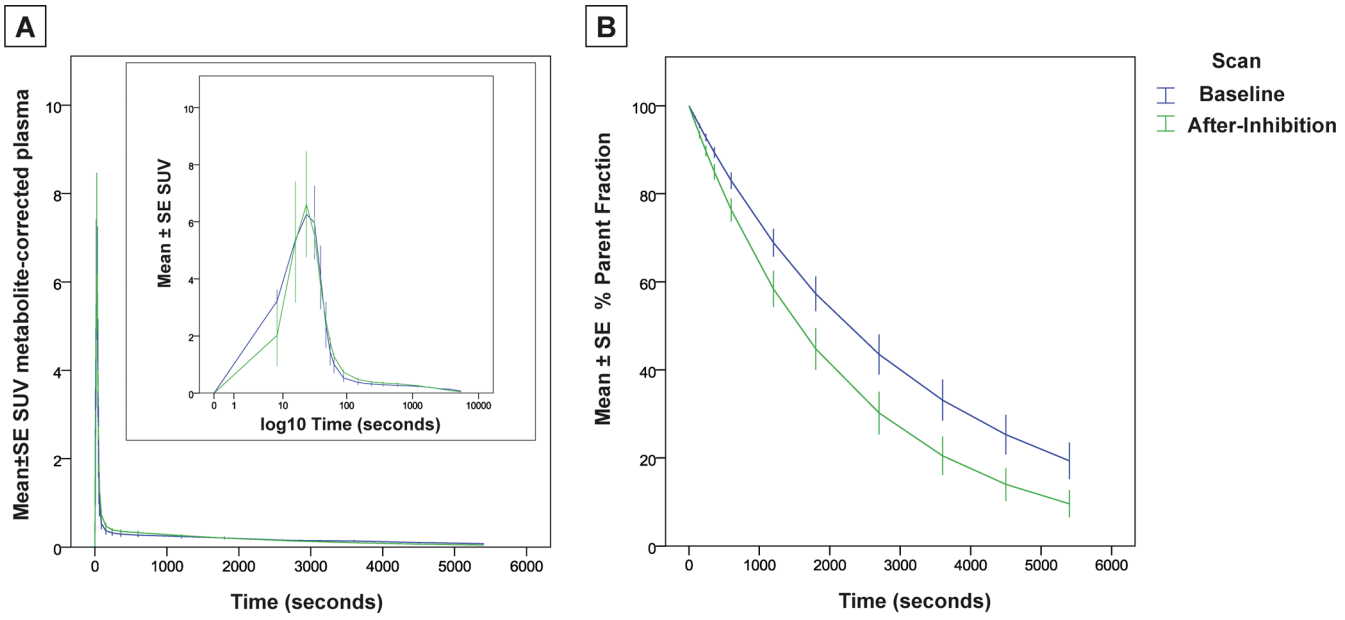

Figure 1. (A) Metabolite-corrected plasma TACs of baseline (blue) and after-inhibition (green) scans (SUV). (B) Percentage of parent fraction at baseline (blue) and after inhibition (green).

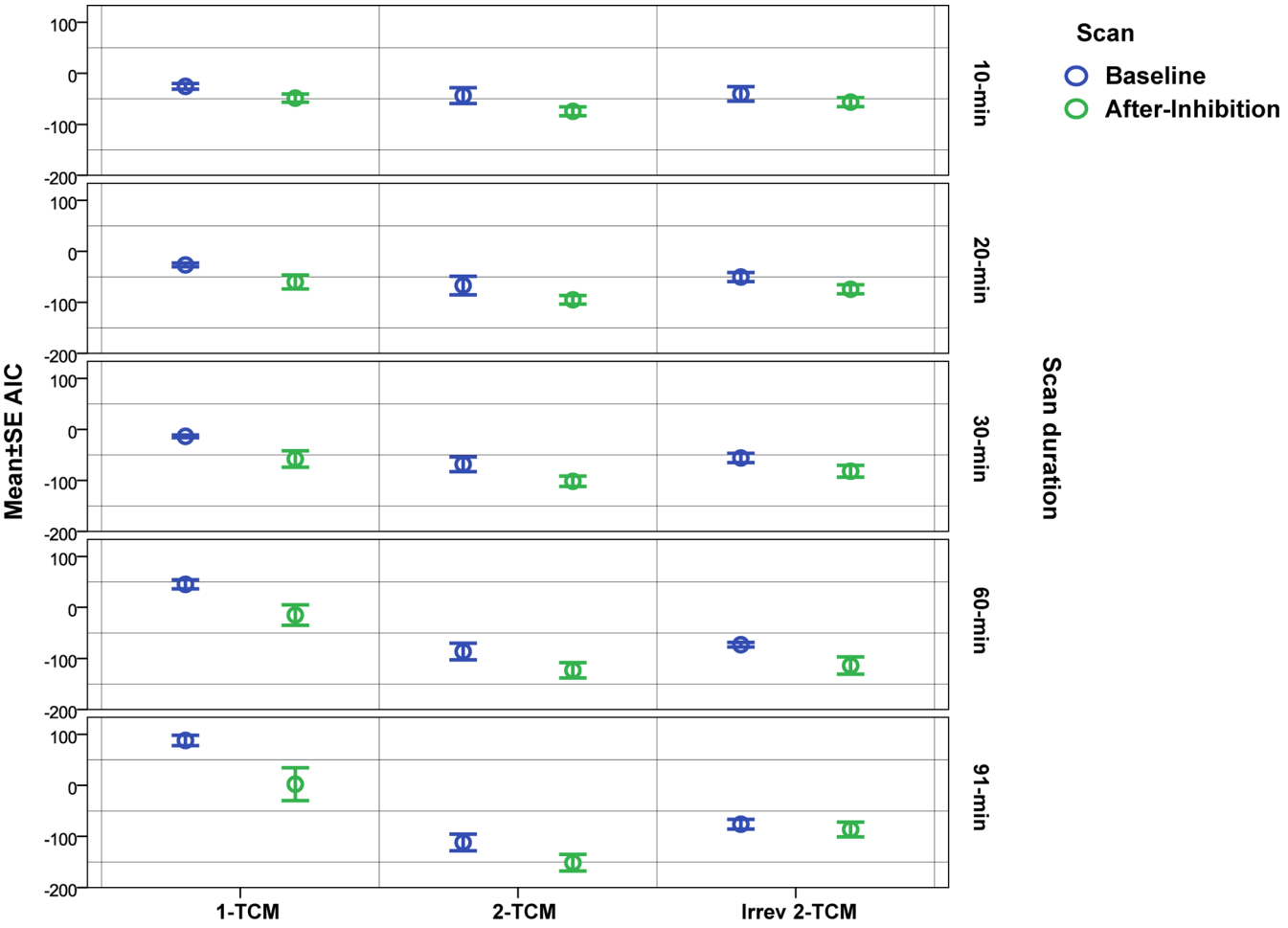

Figure 2. AIC in whole brain using different models for all the scan durations at baseline (blue) and after-inhibition (green) scans. Mean values ± SE are plotted.

inhibition scans to evaluate the effect of inhibition and to select the most appropriate parameter to measure the P-gp function.

2.5. Parametric Images. Parametric images of K_1, V_T, and k_2 at baseline and after inhibition were calculated in one

https://dx.doi.org/10.1021/acs.molpharmaceut.0c01014
Mol. Pharmaceutics XXXX, XXX, XXX−XXX

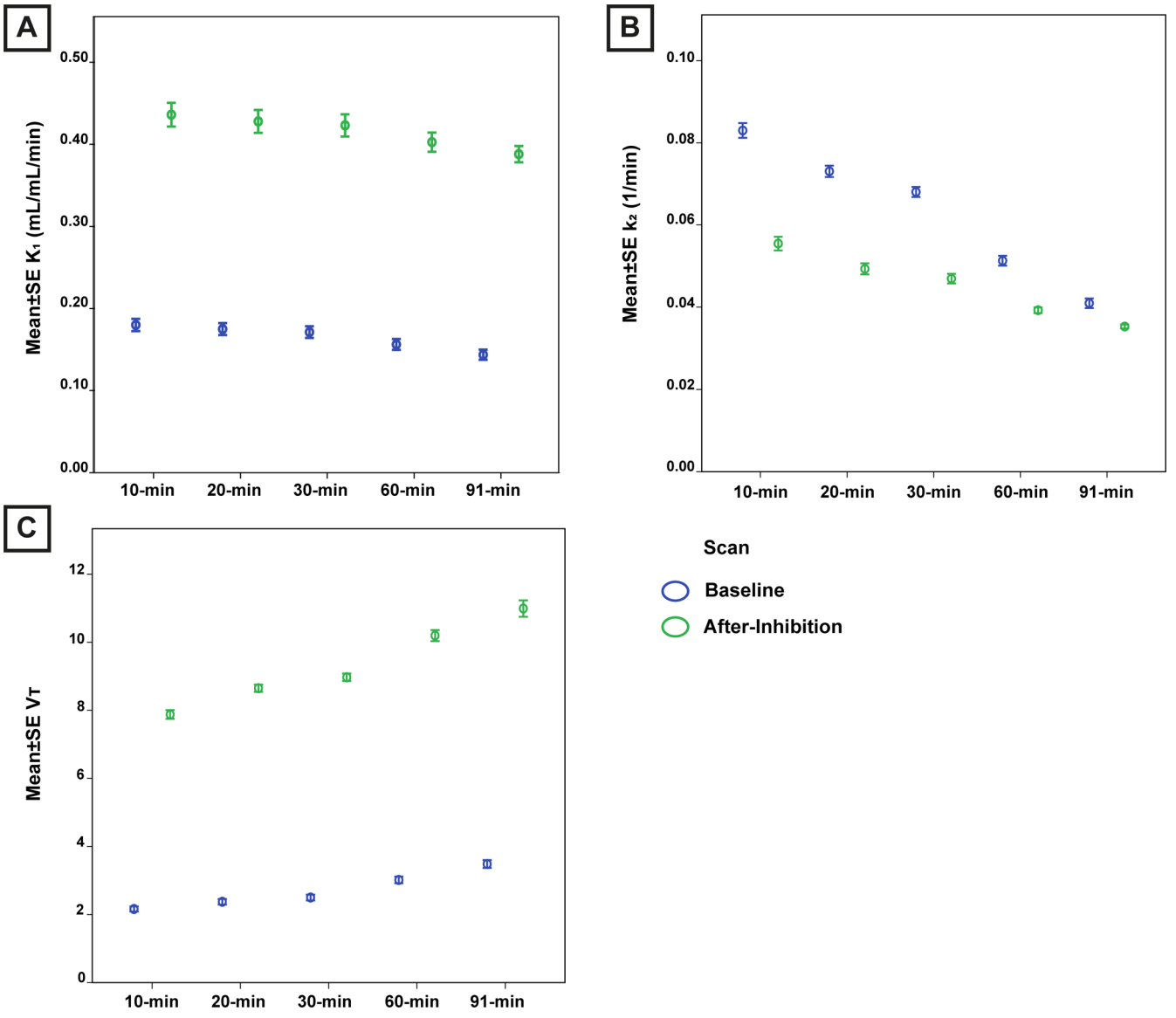

Figure 3. K_1 (A), k_2 (B), and V_T (C) in whole brain at baseline (blue) and after inhibition (green), estimated from scans with different durations. Mean values ± SE are plotted.

monkey (subject 2) for representation purposes. The metabolite-corrected plasma TAC was used as an input function for the basis function implementation of 1-TCM using PMOD v3.8 software.

2.6. Statistical Analysis. Inferential results are reported as estimated marginal mean ± SE (mean ± SE) unless mentioned otherwise. Statistical analysis was performed using IBM SPSS Statistics version 23 (Armonk, NY, USA). Differences in kinetic parameter values and Akaike values among models, scan durations, and type of scans (baseline or after-inhibition) were assessed independently for each brain region by the generalized estimated equation (GEE) model using an independent working correlation matrix.[45,46] The GEE is recommended for the analysis of longitudinal data and it is also more efficient, achieving higher power with a small sample size.[47] The relationship between the estimated parameters calculated with different models and different data sets was explored by linear regression analysis. Results were considered statistically significant at $p < 0.05$, without correction for multiple comparisons. The differences between baseline and after inhibition are reported as a percentage and calculated as follows: 100 × (after-inhibition − baseline)/baseline.

3. RESULTS

3.1. Tracer Production. Molar activities and radiochemical purities of (*R*)-[^{11}C]verapamil productions as well as the mass and radioactive dose injected in each animal are reported in Table 2.

3.2. Input Function and Metabolism of (*R*)-[^{11}C]-verapamil. A significant increase in the area under the curve (AUC) of the whole-blood TACs was found after the administration of the P-gp inhibitor tariquidar (baseline = 2.03 ± 0.33 *vs* after inhibition = 2.22 ± 0.35, $p = 0.041$). No statistically significant differences between baseline and after-inhibition scans were found in the uncorrected or metabolite-corrected plasma TACs (Figure 1). However, a statistically significant reduction of the % parent fraction of (*R*)-[^{11}C]verapamil was found after the P-gp inhibition (75.25 ± 1.37%, $p = 0.019$) compared to baseline values (79.82 ±

https://dx.doi.org/10.1021/acs.molpharmaceut.0c01014
Mol. Pharmaceutics XXXX, XXX, XXX−XXX

Table 3. Changes in V_T, K_1, and k_2 after P-gp Inhibition in Brain Regions using 30 and 91 min Scan Durations and 1-TCM[a]

scan duration	regions	K_1 ± SE (%)	p values	V_T ± SE (%)	p values	k_2 ± SE (%)	p values
		% of Changes between Baseline and after-Inhibition Scan in 30 min Scan					
30 min	basal ganglia	156 ± 45	<0.001	244 ± 38	<0.001	−25 ± −4	<0.001
	brainstem	176 ± 46	<0.001	241 ± 33	<0.001	−19 ± −2	0.008
	cerebellum	141 ± 37	<0.001	276 ± 42	<0.001	−35 ± −4	<0.001
	cingulate cortex	138 ± 32	<0.001	294 ± 41	<0.001	−40 ± −4	<0.001
	orbitofrontal cortex	93 ± 28	<0.001	190 ± 39	<0.001	−33 ± −3	<0.001
	hippocampus	146 ± 35	<0.001	227 ± 32	<0.001	−25 ± −3	<0.001
	hypothalamus	158 ± 44	<0.001	270 ± 39	<0.001	−30 ± −4	<0.001
	insular cortex	152 ± 38	<0.001	294 ± 36	<0.001	−35 ± −5	<0.001
	midbrain	205 ± 57	<0.001	305 ± 49	<0.001	−25 ± −4	<0.001
	occipital cortex	130 ± 29	<0.001	268 ± 35	<0.001	−37 ± −4	<0.001
	parietal cortex	127 ± 31	<0.001	247 ± 34	<0.001	−34 ± −4	<0.001
	striatum	168 ± 45	<0.001	267 ± 40	<0.001	−27 ± −3	<0.001
	temporal cortex	143 ± 41	<0.001	242 ± 39	<0.001	−28 ± −4	<0.001
	thalamus	176 ± 41	<0.001	285 ± 33	<0.001	−28 ± −4	<0.001
	white matter	145 ± 36	<0.001	268 ± 38	<0.001	−33 ± −4	<0.001
	whole brain	136 ± 34	<0.001	252 ± 37	<0.001	−33 ± −4	<0.001
		% of Changes between Baseline and after-Inhibition Scan in 91 min Scan					
91 min	basal ganglia	174 ± 46	<0.001	210 ± 42	<0.001	−11 ± −1	0.059
	brainstem	199 ± 48	<0.001	199 ± 32	<0.001	1 ± 0	0.855
	cerebellum	167 ± 41	<0.001	231 ± 43	<0.001	−18 ± −2	0.013
	cingulate cortex	166 ± 37	<0.001	237 ± 43	<0.001	−21 ± −2	0.041
	orbitofrontal cortex	111 ± 30	<0.001	153 ± 40	<0.001	−16 ± −2	0.049
	hippocampus	162 ± 37	<0.001	198 ± 35	<0.001	−13 ± −2	0.160
	hypothalamus	184 ± 46	<0.001	215 ± 43	<0.001	−9 ± −1	0.224
	insular cortex	177 ± 40	<0.001	246 ± 43	<0.001	−19 ± −2	0.004
	midbrain	228 ± 62	<0.001	267 ± 52	<0.001	−11 ± −2	0.314
	occipital cortex	155 ± 34	<0.001	221 ± 34	<0.001	−20 ± −2	0.018
	parietal cortex	148 ± 34	<0.001	204 ± 36	<0.001	−18 ± −2	0.076
	striatum	193 ± 47	<0.001	220 ± 41	<0.001	−8 ± −1	0.293
	temporal cortex	165 ± 43	<0.001	199 ± 41	<0.001	−10 ± −1	0.112
	thalamus	200 ± 43	<0.001	243 ± 39	<0.001	−12 ± −1	0.222
	white matter	170 ± 39	<0.001	223 ± 41	<0.001	−16 ± −2	0.094
	whole-brain	159 ± 37	<0.001	208 ± 40	<0.001	−15 ± −2	0.072

[a]Mean values ± SE are listed, changes are shown as percentages.

1.26%). The K_e and $T_{1/2}$ of (*R*)-[^{11}C]verapamil did not significantly change after the P-gp inhibition.

3.3. Plasma Input Models: Compartmental Models. *3.3.1. Blood Volume Fraction.* After correcting the whole-blood and plasma TACs for blood delay, the fractional vB was either fixed to 3, 4, 5, 6, and 7% or used as a fit parameter. According to the AIC, the best fits were obtained when vB was used as a fit parameter, which provided values ranging between 4 and 6%. Moreover, the SE % of the estimated parameters was also lower when vB was fitted rather than fixed. Similar results were obtained when vB was fixed to 5%. Supporting Information Figure S1 shows boxplots of AIC values and SE % K_1 values for the whole brain using different scan durations and models. Because fixing vB did not improve the fits, the following analyses have been performed using vB as the fit parameter.

3.3.2. Model Selection for Different Scan Durations. The 1-TCM and 2-TCM fits showed similar AIC values in short scans, but in scans longer than 60 min, the lowest Akaike values were found using 2-TCM. Figure 2 shows the AIC for the whole brain for all tested scan durations and both scans (baseline and after inhibition) obtained with 1-TCM, 2-TCM, and irreversible 2-TCM.

For the 60 min scan, even though the lowest AIC values were found using 2-TCM, the model showed very large SE % (>100%) in the estimation of k_2, k_4, and V_T. For instance, the mean SE % V_T of the whole brain at baseline using 60 min scan duration was 14,898 ± 12,158. Using 2-TCM, the SE % V_T values were in 35 cases (out of 96) higher than 100% and in 22 higher than 1000%. In the case of 91 min scan duration, 2-TCM provided lower AIC values than 1-TCM; however, some regions showed unreliable values. In 13 cases (out of 96), the SE % V_T were higher than 100% and in three cases higher than 1000%. For these reasons, 1-TCM (which showed lower SE %) was selected as the most robust model to analyze the data for all scan durations. Supporting Information Figure S2 shows representative 1-TCM and 2-TCM fits for the 30 and 91 min scans of the whole brain.

3.3.3. Effect of Scan Duration. Based on our findings described above, 1-TCM was used to fit the PET data for all tested scan durations. The evaluated scan durations did not affect significantly K_1 estimations (3−13%), at least during the first 60 min of the scan. However, the estimation of k_2 decreased and the V_T increased with longer scan durations in both baseline and after-inhibition scans. In Figure 3, the effect of scan duration on the kinetic parameters of the whole brain in baseline and after-inhibition scans is shown.

https://dx.doi.org/10.1021/acs.molpharmaceut.0c01014
Mol. Pharmaceutics XXXX, XXX, XXX−XXX

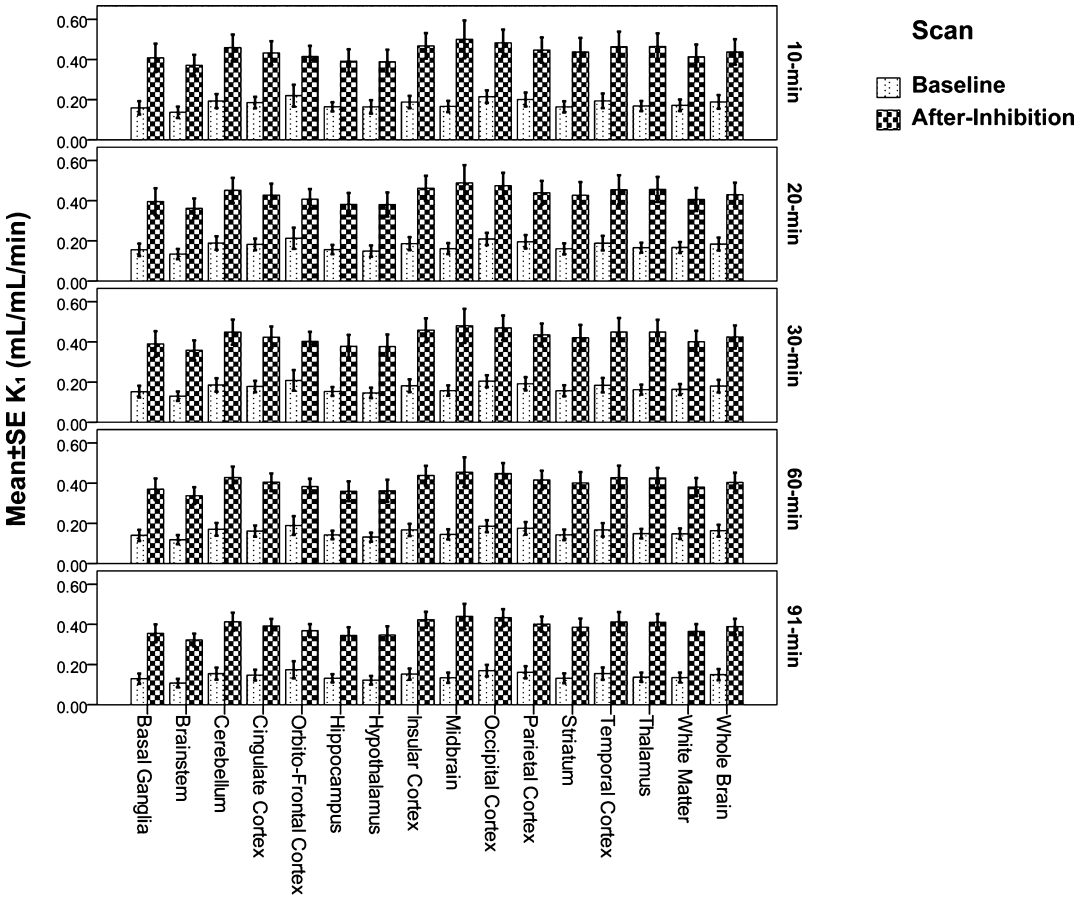

Figure 4. Mean ± SE of K_1 for all brain regions at baseline and after-inhibition scans with different durations.

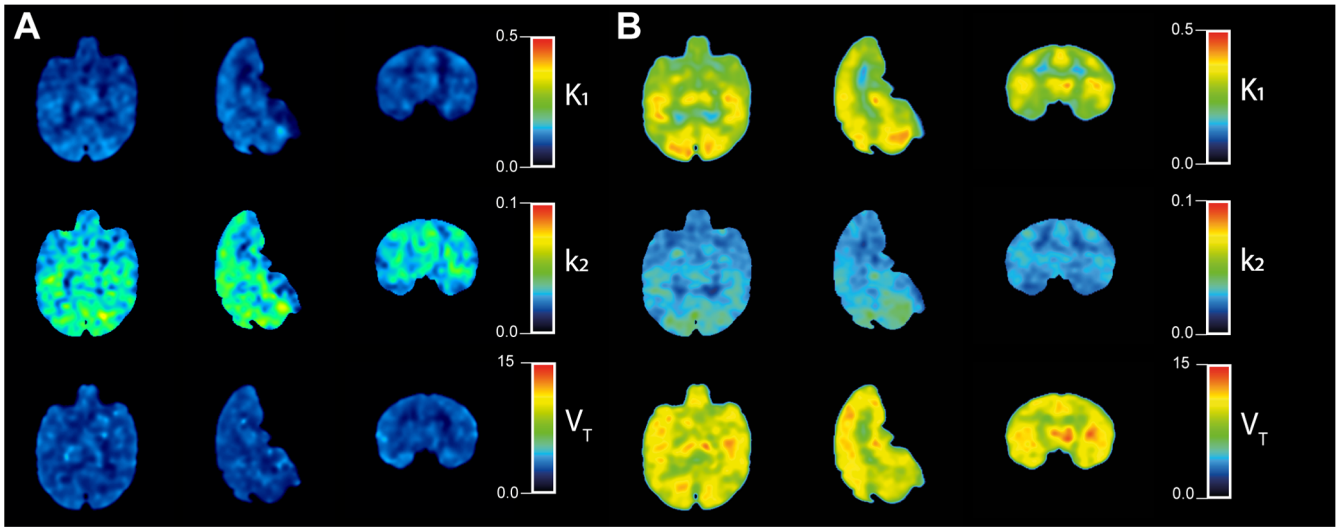

Figure 5. Parametric images of one subject using the 91 min scan data at baseline (A) and after inhibition (B), representing K_1 (mL/cm^3/min, above), k_2 (1/min, center), and V_T (below).

V_T was most affected by the scan duration. In baseline scans, V_T increased by 61% from 2.16 ± 0.24 in a 10 min scan to 3.48 ± 0.38 ($p < 0.001$) in a 91 min scan. Similarly, in after-inhibition scans, the V_T increased by 40% from 7.88 ± 0.20 in 10 min to 10.99 ± 0.85 ($p < 0.001$) in a 91 min scan. The baseline V_T in the 60 min scan also increased by 40% ($p < 0.001$) and in after-inhibition scans by 29% ($p < 0.001$) compared to the values in the 10 min scan. The baseline k_2 decreased by 51% in a 91 min scan and by 36% in after-inhibition scans compared to a 10 min scan.

3.3.4. Effect of P-gp Inhibition. The vB estimated by the model was not significantly different between baseline and after-inhibition scans for any of the scan durations, except for the 10 min scan duration where the estimated vB significantly increased from 0.049 ± 0.001 at baseline to 0.052 ± 0.001 after P-gp inhibition ($p = 0.018$).

https://dx.doi.org/10.1021/acs.molpharmaceut.0c01014
Mol. Pharmaceutics XXXX, XXX, XXX−XXX

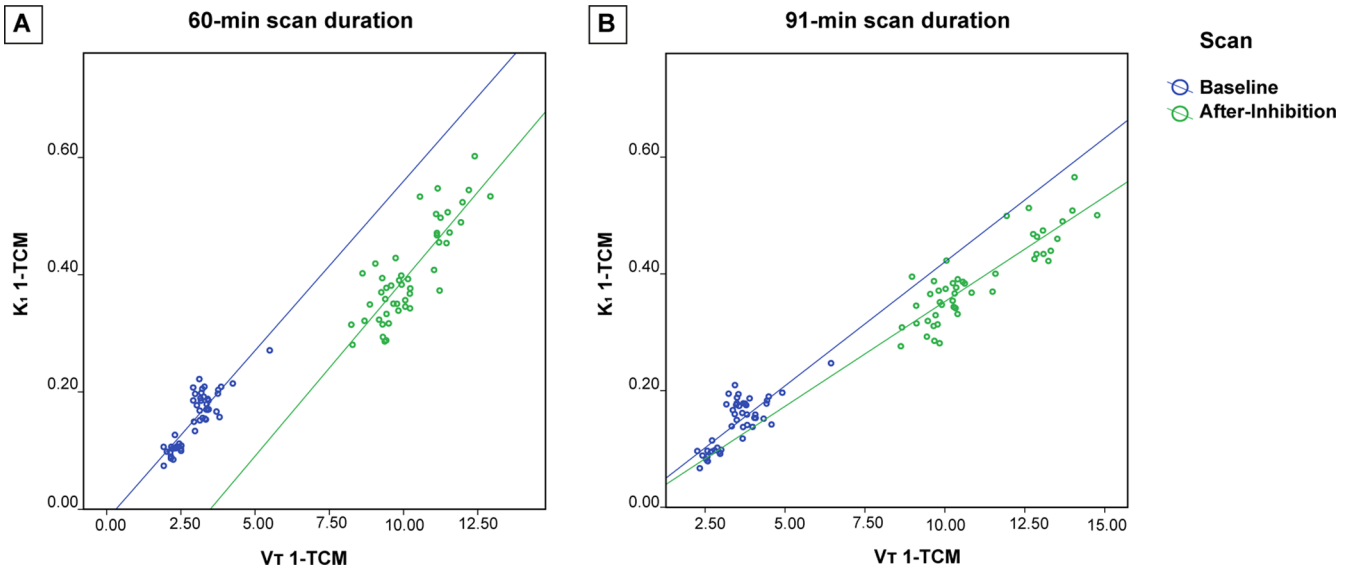

Figure 6. Correlation between K_1 and V_T obtained with 1-TCM using 60 (A) or 91 min (B) data at baseline (blue) and after inhibition (green).

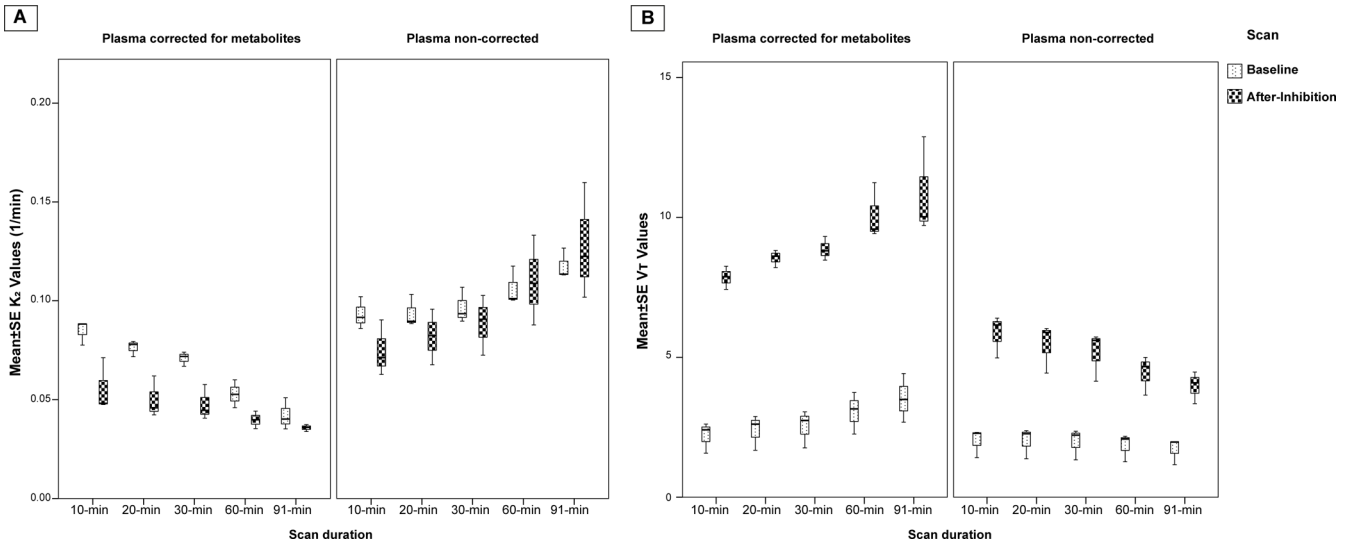

Figure 7. k_2 (A) and V_T (B) at different scan durations at baseline and after inhibition using different input functions (plasma-corrected for radio-metabolites or plasma-non-corrected). Mean values ± SE are plotted.

In all scan durations, the parameter most affected by P-gp inhibition was V_T. In 91 min scans, the whole-brain V_T increased by 208% after P-gp inhibition; meanwhile, the K_1 increased by 159% in after-inhibition scans. The k_2 of the whole brain decreased by 15%. In all scan durations, V_T and K_1 significantly increased in all the brain regions after P-gp inhibition. Meanwhile, k_2 significantly decreased in all scan durations except for the 91 min scan. Table 3 shows the changes in V_T, K_1, and k_2 after the P-gp inhibition in all the brain regions using 30 and 91 min scan durations.

The magnitude of changes is dependent on scan duration because estimated values of V_T and k_2 are different in short and long scans. Figure 4 and Supporting Information Figures S3 and S4 show the mean values of K_1, V_T, and k_2 at baseline and after inhibition.

For illustrative purposes, Figure 5 shows V_T, K_1, and k_2 parametric images of one subject (subject 2) at baseline and after inhibition using 91 min scan and metabolite-corrected plasma as the input function.

3.3.5. Correlation K_1–V_T. In 60 and 91 min scans, K_1 and V_T showed a good correlation at baseline (R^2 = 0.74 and R^2 = 0.61, $p < 0.01$) and after-inhibition scans (R^2 = 0.70 and R^2 = 0.76, $p < 0.01$, respectively). Figure 6 shows the correlation between K_1 and V_T in 60 and 91 min scan for baseline and after-inhibition scans.

3.4. Plasma Non-corrected for Radio-Metabolite Input Models: Compartmental Models. The compartmental analyses were also performed using the plasma radioactivity non-corrected for radio-metabolites as an input function for 1-TCM in all scan durations. For most of the brain regions analyzed, the SE % of K_1, k_2, and V_T was higher when using the plasma radioactivity non-corrected for radio-metabolites than with plasma-corrected for polar radio-metabolites. In 91 min scan durations, the overall SE % V_T was 471% higher than the one obtained with the corrected plasma. Moreover, V_T values obtained with non-corrected plasma were significantly lower than the ones obtained with plasma radioactivity corrected for polar radio-metabolites, especially in after-inhibition scans (*e.g.*,

https://dx.doi.org/10.1021/acs.molpharmaceut.0c01014
Mol. Pharmaceutics XXXX, XXX, XXX−XXX

in 91 min after-inhibition scans V_T non-corrected plasma = 3.97 ± 0.27 *vs.* V_T corrected plasma = 10.87 ± 0.82; $p < 0.001$). The k_2 values obtained with non-corrected plasma were higher than in corrected plasma in both baseline and after-inhibition scans, and the differences were more pronounced at long scan duration (>60 min). For instance, in a 91 min scan, the mean k_2 after inhibition obtained with non-corrected plasma was 0.13 ± 0.014 1/min, and with corrected plasma, it was 0.036 ± 0.001 1/min ($p < 0.001$).

Regarding the effect of scan duration, the estimations of V_T decreased and k_2 increased with the scanning time when plasma non-corrected for radio-metabolites was used as the input function, whereas when plasma radioactivity was corrected for polar radio-metabolites, the estimations of V_T increased and k_2 decreased (see Figure 7). Nevertheless, regarding P-gp inhibition, similar results were obtained compared to the analysis with metabolite-corrected plasma. The administration of tariquidar significantly increased K_1 and V_T at all scan durations. However, the analysis did not find significant changes in k_2 after the P-gp inhibition. At 91 min scan duration, K_1 increased from 0.20 ± 0.03 mL/cm^3/min at baseline to 0.51 ± 0.06 mL/cm^3/min after inhibition ($p < 0.001$) and V_T from 1.71 ± 0.22 at baseline to 3.97 ± 0.27 after P-gp inhibition ($p < 0.001$).

4. DISCUSSION

The aim of this study was to evaluate the kinetics of the P-gp tracer (*R*)-[^{11}C]verapamil in baseline conditions and after P-gp inhibition in nonhuman primates. Moreover, the study also evaluates the kinetics at different acquisition times (10 to 91 min) to assess the effect of the scan duration on the estimated parameters. Our results showed that 1-TCM with fractional vB as a fit parameter is the most suitable compartment model to fit the data at baseline and after-inhibition conditions for all the scan durations tested.

Model preferences seem not to be influenced by the scan duration. Although in the case of long scan durations (>60 min), the lowest AIC were seen with 2-TCM, large SE % (>100%) of the estimated parameters (V_T, k_2, and k_4) were found. These large SE % did not provide reliable V_T values in several brain regions using 60 and 91 min scan durations. Several adjustments were applied to the model fit in an attempt to solve this problem. For instance, the use of 2-TCM while fixing the ratio K_1/k_2 to the whole brain gray matter value, as was suggested for the analysis of (*R*)-[^{11}C]verapamil in humans,[19] or by imposing a lower boundary for the k_4 (0.001 1/min). However, none of these strategies improved the quality of the 2-TCM fit (results not reported). We have also tested a 2-input-compartmental model where we applied both a parent tracer and radio-metabolites plasma input curve at the same time in the model. This model has been already used in previous studies to account for the entrance of radio-metabolites of [^{11}C]verapamil in the brain.[48] However, when using this model, we found large uncertainties in the estimated kinetic parameters (K_1, k_2, and V_T) (with SE % > 100%) in most of the brain regions analyzed (data not shown). The 2-input model did not provide reliable and robust results for our data and was therefore not explored in our paper. Therefore, 1-TCM was selected as the model of choice to analyze the (*R*)-[^{11}C]verapamil data in nonhuman primates for all tested scan durations and for both baseline and after-inhibition scans.

Although different kinetic analysis methods have been previously studied, a clear consensus regarding the optimal method has not yet been reached.[14,19,23,49] In rats, 2-TCM showed better fits than 1-TCM for both baseline and after tariquidar administration scans. Thus, it was selected as the model of choice using either plasma-corrected for polar radio-metabolites or plasma non-corrected for radio-metabolites.[22,50] In humans, several approaches have been applied to fit the (*R*)-[^{11}C]verapamil data.[14] In healthy subjects, 1-TCM with vB as a fit parameter and using a metabolite-corrected plasma input function showed an adequate fit. 2-TCM was also applied; however, the fit did not provide robust parameters.[18] Next, (*R*)-[^{11}C]verapamil was also assessed after the administration of tariquidar (P-gp after-inhibition scans); in this case, a 2-TCM fit was preferred, whereas the data from baseline scans (before the P-gp inhibition) was fitted with 1-TCM using a plasma input function corrected for polar radio-metabolites.[23] Muzi *et al.* used 1-TCM to fit the 10 min scan duration data and 2-TCM for the 45 min scan for both baseline and after P-gp inhibition scans and corrected the plasma input function for polar and lipophilic radio-metabolites. In this study, Muzi *et al.* recommended the use of 10 min scan data to avoid the interference of radio-metabolites with the brain signal.[49] Also, in humans, the use of constrained 2-TCM (*i.e.*, fixing the ratio K_1/k_2 to the mean whole-brain gray matter value) was proposed, with plasma-corrected for polar radio-metabolites as the input function. The results of this analysis suggested that constrained 2-TCM leads to more reproducible results in healthy volunteers.[19]

In our study, the administration of the P-gp inhibitor tariquidar caused a significant increase of V_T and K_1 in all the brain regions analyzed. V_T was the parameter most affected by P-gp inhibition. Tariquidar treatment caused an increase in V_T of 257% ($p < 0.001$) in the 10 min scan, of 230% ($p < 0.001$) in the 60 min scan, and an increase of 208% ($p < 0.001$) in 91 min scan compared to baseline. K_1 was also affected by P-gp inhibition. The changes in whole-brain K_1 between baseline and after-inhibition scans varied from 131% in 10 min scans to 159% in 91 min scans. Moreover, we also found a significant reduction in whole-brain k_2 at all the scan durations except for the 91 min scan. k_2 was decreased by 34% in 10 min ($p < 0.001$) scans and by 15% in 91 min scans ($p = 0.072$). These results support the ability of (*R*)-[^{11}C]verapamil to detect changes in the P-gp function in nonhuman primates as has been already proven in other species.

Various studies have been done in humans under baseline and inhibition conditions.[23,24] Three hours after the administration of 2 mg/kg of tariquidar by intravenous infusion over 30 min caused an increase of V_T and K_1 by 24 ± 15 and 49 ± 36%, respectively.[23] Another study found that the administration of tariquidar as a continuous infusion during 1 h before the PET scan and during the 60 min PET scan (total infusion time 2 h and mean tariquidar dose 5.9 ± 1.0 mg/kg) increased V_T and K_1 values by 273 ± 78 and 259 ± 74%, respectively, relative to baseline scans.[24] Although the inhibition of the P-gp function also caused an increase in the K_1 and V_T values in humans, the values of the kinetic parameters, and the effect size are different from the monkeys' values. However, because different doses of tariquidar, routes of administration, and duration of the perfusion were used in the monkeys, the human and monkey values cannot be directly compared. In rats, the P-gp inhibition also caused an increase in K_1 and V_T, but similar discrepancies were observed.[22,50]

Previous studies have shown that lipophilic radio-metabolites of (*R*)-[^{11}C]verapamil have similar kinetics as the parent

https://dx.doi.org/10.1021/acs.molpharmaceut.0c01014
Mol. Pharmaceutics XXXX, XXX, XXX−XXX

tracer; thus, most of the studies use the radiotracer concentration in plasma-corrected for polar radio-metabolites as the input function for the kinetic analysis.[18,51] Our kinetic analysis was performed using the radiotracer concentration in plasma-corrected for polar radio-metabolites and non-corrected for radio-metabolites as the input function. When plasma non-corrected for radio-metabolites was used, large SE % (>50%) in the parameter estimations was found. Therefore, corrections for polar radio-metabolites should be performed to avoid noisy data and low reliability of the estimated parameters. For long scan durations, V_T values calculated with plasma non-corrected for radio-metabolites as input were lower (40−60%) than with corrected plasma input, and k_2 values were 100−260% higher. These lower V_T values and the decrease in V_T estimations with increasing scan durations may be caused by the higher radioactivity concentration in the input function. Therefore, if the radioactivity in blood is not corrected by the amount of radio-metabolites, the model underestimates the V_T values. When plasma-corrected for metabolites are used as the input function, the estimated V_T should not vary with the scan duration. However, because the plasma was only corrected by polar metabolites, it can be that lipophilic metabolites also accumulate in the brain, which may cause the increase in the V_T estimations with longer scan durations. Concerning the tariquidar administration, the analysis using non-corrected plasma input showed a significant increase in V_T and K_1 after P-gp inhibition as was also observed when plasma-corrected for polar radio-metabolites was used. In 91 min scans, V_T increased up to 132% ($p < 0.001$) in after-inhibition scans relative to baseline and K_1 up to 150% ($p < 0.001$). This similar effect of P-gp inhibition on K_1 and V_T may allow avoiding the radio-metabolite analysis, which is considered as a time-consuming and tedious process. However, if changes in the metabolism of (*R*)-[^{11}C]verapamil occur due to a disease condition or administration of treatments, the kinetic quantification can be incorrect. Therefore, the correction of plasma radioactivity for polar radio-metabolites, which have different kinetics than the parent fraction, should be performed, as was also concluded from human studies.[18]

Our baseline V_T values using either metabolite-corrected or non-corrected plasma inputs were higher than those obtained with rats.[22,50] However, K_1 values in rats and nonhuman primates at baseline conditions were similar. In our study, the mean whole-brain K_1 value at baseline was 0.15 ± 0.02 mL/cm^3/min in 91 min scans using plasma-corrected for radio-metabolites, whereas in rats, the K_1 values calculated with 2-TCM and plasma-corrected for polar radio-metabolites were 0.16 ± 0.05 mL/cm^3/min.[50] Compared with human data, the K_1 and V_T values obtained in our study were also higher. The baseline K_1 values in humans were 0.034 ± 0.009 mL/cm^3/min and increased to 0.049 ± 0.009 mL/cm^3/min after P-gp inhibition. The V_T values in 40 min scans were 0.65 ± 0.13 at baseline and 0.80 ± 0.07 after inhibition, as calculated with 2-TCM.[23] Compared with our 30 min scan duration data, baseline K_1 values in nonhuman primates were 429% higher relative to humans, and the baseline V_T values were 288% higher. These different values could be caused by species differences in the expression of P-gp at the BBB.[52,53]

Kinetic evaluation of another strong P-gp substrate tracer, [^{11}C]-*N*-desmethyl-loperamide ([^{11}C]dLop), in nonhuman primates before and after administration of the P-gp inhibitor cyclosporine A,[54] showed similar increases of brain uptake after P-gp inhibition as were observed in our study. The evaluation of [^{11}C]dLop did not use compartmental models and, therefore, the brain uptake was not calculated using the V_T but using the ratio between the AUC from the brain and the AUC from the blood (AUCR = AUC_{brain}/AUC_{blood}).[54] In this study, the AUCR after the administration of the P-gp inhibitor (15 mg/kg/h i.v.) was enhanced to 10.8 ± 3.6,[54] which is similar to our after-inhibition V_T value of the whole brain of 10.87 ± 0.82.

With regard to the tracer kinetics in plasma, it is known that (*R*)-[^{11}C]verapamil suffers from extensive *in vivo* metabolism, both in small animals and in humans. In the present study on nonhuman primates, the percentage of parent tracer at 30 min after the injection was 57% in baseline scans and 45% in after-inhibition scans, after correction for polar radio-metabolites. Regarding the differences in parent tracer between baseline and after-inhibition scans, our analysis found a significant reduction (6%) in the percentage of parent (*R*)-[^{11}C]verapamil in after-inhibition scans compared to baseline. In humans, the percentage of parent tracer is around 45% at 1 h after the injection.[18] In rats, at 30 min after tracer injection, the fraction of parent (*R*)-[^{11}C]verapamil in plasma was 47%, and after 1 h, it was 27%.[55] Previous radio-metabolite studies with nonhuman primates, performed by high-performance liquid chromatography, have already reported a strong metabolism of (*R*)-[^{11}C]verapamil with around 80% of plasma radioactivity associated with radio-metabolites (polar and lipophilic radio-metabolites) at 30 min after the injection.[35] Therefore, the rate of metabolism of (*R*)-[^{11}C]verapamil appears to be rapid and similar in different species.

Short PET scan durations are more convenient for the subjects and also to simplify the kinetic evaluation by reducing the impact of tracer metabolism. In our study, K_1 values slightly decreased (3−13%) with increasing scan duration but remained relatively constant regardless of the scan duration applied. V_T was most affected by the scan duration. In the 91 min scan, V_T increased up to 61% ($p < 0.001$) in baseline and 40% ($p < 0.001$) in after-inhibition scans compared to the values obtained with 10 min scan duration. We also observed a decrease in k_2 values (by 51% in baseline and 36% after inhibition) with increasing scan durations. This coupled increase in the V_T and decrease in the k_2 estimations might be caused by the accumulation of radio-metabolites in the brain. As was found for rats and humans, radio-metabolites formed by the metabolism of (*R*)-[^{11}C]verapamil can cross the BBB and accumulate inside the brain. This fact may complicate the kinetic analysis of the tracer because it is not possible to differentiate the origin of the radioactive signal (radio-metabolites or parent tracer). Thus, short PET acquisition times have been proposed for the analysis of (*R*)-[^{11}C]-verapamil.[14,49,55] Because K_1 is less affected by the scan duration than V_T, we recommend the use of K_1 calculated using 1-TCM and short PET scan durations to measure the P-gp function at the BBB of nonhuman primates, preferably accomplished with quantitative perfusion PET studies, allowing to differentiate between P-gp function and perfusion changes.

A potential limitation of our study is the small sample size, though the longitudinal design may reduce the subject variability and the outcomes show strong and similar inhibitory effects in all the subjects which emphasize the robustness of our results. It is also unfortunate that the study did not analyze lipophilic radio-metabolites in the blood samples. However, this analysis would require larger volumes of blood during

https://dx.doi.org/10.1021/acs.molpharmaceut.0c01014
Mol. Pharmaceutics XXXX, XXX, XXX−XXX

blood sampling, which could be harmful to the animals and lead to errors in the pharmacokinetic analysis. An additional limitation is the position of the animals in the PET scan. In our study, the animals were sitting in the PET scan, whereas in conventional PET scanners, the subjects used to be in a supine position. This fact may change the biological function of the animals and thus alter the kinetics of the tracer. Therefore, the kinetic comparison with other PET studies must be interpreted with caution. However, this position enables the performance of the PET scans in conscious unanesthetized monkeys; thus, anesthetics will not interfere in the distribution of the tracer.[56] Moreover, our study did not correct for partial volume effect; thus, the radioactivity of some small brain regions may be affected by spillover from regions with high tracer uptake.

This study has provided more insights into the pharmacokinetic parameters of (*R*)-[^{11}C]verapamil in nonhuman primates, allowing the comparison with other species. Moreover, these results enable the head-to-head comparison of the properties of a novel P-gp PET tracer, such as [^{18}F]MC225[37] or [^{11}C]metoclopramide,[31] with the P-gp tracer, (*R*)-[^{11}C]-verapamil, in nonhuman primates, a species larger than rodents and physiologically more similar to humans.[57]

5. CONCLUSIONS

Our results suggest that 1-TCM is the model of choice to analyze the PET data of (*R*)-[^{11}C]verapamil in nonhuman primates. The model preference is not affected by scan duration, and a similar approach should be used in baseline scans when the P-gp function is fully functional and in scans after P-gp inhibition. V_T and K_1 values obtained in nonhuman primates were different from humans and rats with the same radiotracer, which highlights P-gp expression differences among species. However, the rate of (*R*)-[^{11}C]verapamil metabolism seems similar in all the species examined. V_T was the parameter most affected by the challenge (P-gp inhibition). However, because the estimated V_T changes with scan duration and thus cannot be reliably determined, we recommend the use of K_1 calculated with 1-TCM as a suitable parameter to measure the P-gp function at the BBB of nonhuman primates. Moreover, short scan durations are recommended to avoid quantification being affected by the presence of radiometabolites in the brain.

■ ASSOCIATED CONTENT

Supporting Information

The Supporting Information is available free of charge at https://pubs.acs.org/doi/10.1021/acs.molpharmaceut.0c01014.

Boxplot of whole-brain AIC values and SE % K_1 values using different vBs at different models, scan durations, and type of scan; representative 1-TCM and 2-TCM of one subject using 30 and 91 min scan duration at baseline and after inhibition; mean ± SE of k_2 of all the brain regions at baseline and after-inhibition scans using different scan durations; and mean ± SE of V_T of all the brain regions at baseline and after-inhibition scans using different scan durations (PDF)

■ AUTHOR INFORMATION

Corresponding Author

Gert Luurtsema − *Department of Nuclear Medicine and Molecular Imaging, University of Groningen, University Medical Center Groningen, Groningen 9713 GZ, The Netherlands*; Email: g.luurtsema@umcg.nl

Authors

Lara García-Varela − *Department of Nuclear Medicine and Molecular Imaging, University of Groningen, University Medical Center Groningen, Groningen 9713 GZ, The Netherlands*; orcid.org/0000-0001-9803-4708

David Vállez García − *Department of Nuclear Medicine and Molecular Imaging, University of Groningen, University Medical Center Groningen, Groningen 9713 GZ, The Netherlands*

Takeharu Kakiuchi − *Central Research Laboratory, Hamamatsu Photonics KK, Hamamatsu 434-8601, Shizuoka, Japan*

Hiroyuki Ohba − *Central Research Laboratory, Hamamatsu Photonics KK, Hamamatsu 434-8601, Shizuoka, Japan*

Shingo Nishiyama − *Central Research Laboratory, Hamamatsu Photonics KK, Hamamatsu 434-8601, Shizuoka, Japan*

Tetsuro Tago − *Research Team for Neuroimaging, Tokyo Metropolitan Institute of Gerontology, Tokyo 173-0015, Japan*; orcid.org/0000-0002-9545-0922

Philip H. Elsinga − *Department of Nuclear Medicine and Molecular Imaging, University of Groningen, University Medical Center Groningen, Groningen 9713 GZ, The Netherlands*

Hideo Tsukada − *Central Research Laboratory, Hamamatsu Photonics KK, Hamamatsu 434-8601, Shizuoka, Japan*

Nicola A. Colabufo − *Department of Pharmacy, University of Bari Aldo Moro, Bari 70125, Italy; Biofordrug, Spin-off Università degli Studi di Bari "A. Moro", Bari 70019, Italy*; orcid.org/0000-0001-5639-7746

Rudi A.J.O. Dierckx − *Department of Nuclear Medicine and Molecular Imaging, University of Groningen, University Medical Center Groningen, Groningen 9713 GZ, The Netherlands*

Aren van Waarde − *Department of Nuclear Medicine and Molecular Imaging, University of Groningen, University Medical Center Groningen, Groningen 9713 GZ, The Netherlands*

Jun Toyohara − *Research Team for Neuroimaging, Tokyo Metropolitan Institute of Gerontology, Tokyo 173-0015, Japan*

Ronald Boellaard − *Department of Nuclear Medicine and Molecular Imaging, University of Groningen, University Medical Center Groningen, Groningen 9713 GZ, The Netherlands*

Complete contact information is available at: https://pubs.acs.org/10.1021/acs.molpharmaceut.0c01014

Author Contributions

L.G.-V. registered the PET images with the corresponding MRI images, did the pharmacokinetic analysis, and wrote the manuscript with help from all authors. D.V.G. contributed to the data analysis and the preparation of the manuscript. T.K. and H.O. performed the preclinical studies. S.N. and T.T. synthesized the tracer. P.H.E. commented on the final manuscript. H.T. supervised the nonhuman primate PET study. N.A.C., R.A.J.O.D., and A.v.W. commented on the final manuscript. J.T. synthesized the tracer and contributed to the design of the preclinical experiments. R.B. contributed to the design of the pharmacokinetic analysis, helped with the

https://dx.doi.org/10.1021/acs.molpharmaceut.0c01014
Mol. Pharmaceutics XXXX, XXX, XXX−XXX

interpretation of the data and the preparation of the manuscript. G.L. contributed to the design of the preclinical experiments and helped in the interpretation of the data and the preparation of the manuscript. All authors read and approved the final manuscript.

Notes

The authors declare no competing financial interest.

The data sets used and analyzed during the current study are available from the corresponding author on reasonable request.

■ ABBREVIATIONS

[^{11}C]dLop, [^{11}C]-*N*-desmethyl-loperamide; 1-TCM, 1-tissue compartment model; 2-TCM, 2-tissue compartmental model; ABC transporters, ATP binding cassette transporter; AIC, Akaike information criterion; AUC, area under the curve; BBB, blood−brain barrier; CNS, central nervous system; EMM, estimated marginal mean; GEE, generalized estimated equation; Irrev 2-TCM, irreversible 2-tissue compartmental model; K_1, influx constant; k_2, efflux constant; K_e, rate of tracer elimination; PET, positron emission tomography; P-gp, P-glycoprotein; SE %, percentage standard errors of estimated parameters; SE, standard error; SUV, standardized uptake value; $T_{1/2}$, biological half-life; TAC, time−activity curves; vB, blood volume; VOI, volumes-of-interest; V_T, volume of distribution

■ REFERENCES

(1) McTavish, D.; Sorkin, E. M. Verapamil. *Drugs* **1989**, *38*, 19−76.

(2) Elsinga, P. H.; Franssen, E. J.; Hendrikse, N. H.; Fluks, L.; Weemaes, A. M.; van der Graaf, W. T.; de Vries, E. G.; Visser, G. M.; Vaalburg, W. Carbon-11-Labeled Daunorubicin and Verapamil for Probing P-Glycoprotein in Tumors with PET. *J. Nucl. Med.* **1996**, *37*, 1571−1575.

(3) Hendrikse, N. H.; de Vries, E. G. E.; Franssen, E. J. F.; Vaalburg, W.; van der Graaf, W. T. A. In Vivo Measurement of [11C]Verapamil Kinetics in Human Tissues. *Eur. J. Clin. Pharmacol.* **2001**, *56*, 827−829.

(4) Linton, K. J.; Higgins, C. F. Structure and Function of ABC Transporters: The ATP Switch Provides Flexible Control. *Pflugers Arch.* **2007**, *453*, 555−567.

(5) Abbott, N. J.; Patabendige, A. A. K.; Dolman, D. E. M.; Yusof, S. R.; Begley, D. J. Structure and Function of the Blood-Brain Barrier. *Neurobiol. Dis.* **2010**, *37*, 13−25.

(6) Löscher, W.; Potschka, H. Role of Drug Efflux Transporters in the Brain for Drug Disposition and Treatment of Brain Diseases. *Prog. Neurobiol.* **2005**, *76*, 22−76.

(7) de Klerk, O. L.; Willemsen, A. T. M.; Roosink, M.; Bartels, A. L.; Harry Hendrikse, N.; Bosker, F. J.; den Boer, J. A. Locally Increased P-Glycoprotein Function in Major Depression: A PET Study with [11C]Verapamil as a Probe for P-Glycoprotein Function in the Blood-Brain Barrier. *Int. J. Neuropsychopharmacol.* **2009**, *12*, 895−904.

(8) de Klerk, O. L.; Willemsen, A. T. M.; Bosker, F. J.; Bartels, A. L.; Hendrikse, N. H.; den Boer, J. A.; Dierckx, R. A. Regional Increase in P-Glycoprotein Function in the Blood-Brain Barrier of Patients with Chronic Schizophrenia:. A PET Study with [11C]Verapamil as a Probe for P-Glycoprotein Function. *Psychiatry Res., Neuroimaging* **2010**, *183*, 151−156.

(9) Mahringer, A.; Fricker, G. ABC Transporters at the Blood-Brain Barrier. *Expert Opin. Drug Metab. Toxicol.* **2016**, *12*, 499−508.

(10) Toyohara, J. Importance of P-Gp PET Imaging in Pharmacology. *Curr. Pharm. Des.* **2016**, *22*, 5830−5836.

(11) Luurtsema, G.; Elsinga, P.; Dierckx, R.; Boellaard, R.; Waarde, A. PET Tracers for Imaging of ABC Transporters at the Blood-Brain Barrier: Principles and Strategies. *Curr. Pharm. Des.* **2016**, *22*, 5779−5785.

(12) Tournier, N.; Stieger, B.; Langer, O. Imaging Techniques to Study Drug Transporter Function in Vivo. *Pharmacol. Ther.* **2018**, *189*, 104−122.

(13) Syvänen, S.; Eriksson, J. Advances in PET Imaging of P-Glycoprotein Function at the Blood-Brain Barrier. *ACS Chem. Neurosci.* **2013**, *4*, 225−237.

(14) Lubberink, M. Kinetic Models for Measuring P-Glycoprotein Function at the Blood-Brain Barrier with Positron Emission Tomography. *Curr. Pharm. Des.* **2016**, *22*, 5786−5792.

(15) Langer, O.; Bauer, M.; Hammers, A.; Karch, R.; Pataraia, E.; Koepp, M. J.; Abrahim, A.; Luurtsema, G.; Brunner, M.; Sunder-Plassmann, R.; Zimprich, F.; Joukhadar, C.; Gentzsch, S.; Dudczak, R.; Kletter, K.; Müller, M.; Baumgartner, C. Pharmacoresistance in Epilepsy: A Pilot PET Study with the P-Glycoprotein Substrate R-[11C]Verapamil. *Epilepsia* **2007**, *48*, 1774−1784.

(16) van Assema, D. M. E.; Lubberink, M.; Bauer, M.; van der Flier, W. M.; Schuit, R. C.; Windhorst, A. D.; Comans, E. F. I.; Hoetjes, N. J.; Tolboom, N.; Langer, O.; Müller, M.; Scheltens, P.; Lammertsma, A. A.; van Berckel, B. N. M. Blood−Brain Barrier P-Glycoprotein Function in Alzheimer's Disease. *Brain* **2012**, *135*, 181−189.

(17) Kortekaas, R.; Leenders, K. L.; Van Oostrom, J. C. H.; Vaalburg, W.; Bart, J.; Willemsen, A. T. M.; Hendrikse, N. H. Blood-Brain Barrier Dysfunction in Parkinsonian Midbrain in Vivo. *Ann. Neurol.* **2005**, *57*, 176−179.

(18) Lubberink, M.; Luurtsema, G.; van Berckel, B. N.; Boellaard, R.; Toornvliet, R.; Windhorst, A. D.; Franssen, E. J.; Lammertsma, A. A. Evaluation of Tracer Kinetic Models for Quantification of P-Glycoprotein Function Using (R)-[11C]Verapamil and PET. *J. Cereb. Blood Flow Metab.* **2007**, *27*, 424−433.

(19) van Assema, D. M.; Lubberink, M.; Boellaard, R.; Schuit, R. C.; Windhorst, A. D.; Scheltens, P.; van Berckel, B. N.; Lammertsma, A. A. Reproducibility of Quantitative (R)-[11C]Verapamil Studies. *EJNMMI Res.* **2012**, *2*, 1.

(20) Hendrikse, N. H.; Schinkel, A. H.; De Vries, E. G. E.; Fluks, E.; Van der Graaf, W. T. A.; Willemsen, A. T. M.; Vaalburg, W.; Franssen, E. J. F. Complete in Vivo Reversal of P-Glycoprotein Pump Function in the Blood-Brain Barrier Visualized with Positron Emission Tomography. *Br. J. Pharmacol.* **1998**, *124*, 1413−1418.

(21) Luurtsema, G.; Molthoff, C. F. M.; Windhorst, A. D.; Smit, J. W.; Keizer, H.; Boellaard, R.; Lammertsma, A. A.; Franssen, E. J. F. (R)- and (S)-[11C]Verapamil as PET-Tracers for Measuring P-Glycoprotein Function: In Vitro and in Vivo Evaluation. *Nucl. Med. Biol.* **2003**, *30*, 747−751.

(22) Bankstahl, J. P.; Kuntner, C.; Abrahim, A.; Karch, R.; Stanek, J.; Wanek, T.; Wadsak, W.; Kletter, K.; Muller, M.; Loscher, W.; Langer, O. Tariquidar-Induced P-Glycoprotein Inhibition at the Rat Blood-Brain Barrier Studied with (R)-11C-Verapamil and {PET}. *J. Nucl. Med.* **2008**, *49*, 1328−1335.

(23) Wagner, C. C.; Bauer, M.; Karch, R.; Feurstein, T.; Kopp, S.; Chiba, P.; Kletter, K.; Loscher, W.; Muller, M.; Zeitlinger, M.; Langer, O. A Pilot Study to Assess the Efficacy of Tariquidar to Inhibit P-Glycoprotein at the Human Blood-Brain Barrier with (R)-11C-Verapamil and PET. *J. Nucl. Med.* **2009**, *50*, 1954−1961.

(24) Bauer, M.; Karch, R.; Zeitlinger, M.; Philippe, C.; Römermann, K.; Stanek, J.; Maier-Salamon, A.; Wadsak, W.; Jäger, W.; Hacker, M.; Müller, M.; Langer, O. Approaching Complete Inhibition of P-Glycoprotein at the Human Blood-Brain Barrier: An (R)-[11C]Verapamil PET Study. *J. Cereb. Blood Flow Metab.* **2015**, *35*, 743−746.

(25) Langer, O. Use of PET Imaging to Evaluate Transporter-Mediated Drug-Drug Interactions. *J. Clin. Pharmacol.* **2016**, *56*, S143−S156.

(26) Savolainen, H.; Windhorst, A. D.; Elsinga, P. H.; Cantore, M.; Colabufo, N. A.; Willemsen, A. T.; Luurtsema, G. Evaluation of [18F]MC225 as a PET Radiotracer for Measuring P-Glycoprotein Function at the Blood-Brain Barrier in Rats: Kinetics, Metabolism, and Selectivity. *J. Cereb. Blood Flow Metab.* **2017**, *37*, 1286−1298.

(27) Pottier, G.; Marie, S.; Goutal, S.; Auvity, S.; Peyronneau, M.-A.; Stute, S.; Boisgard, R.; Dolle, F.; Buvat, I.; Caille, F.; Tournier, N.

https://dx.doi.org/10.1021/acs.molpharmaceut.0c01014
Mol. Pharmaceutics XXXX, XXX, XXX−XXX

Imaging the Impact of the P-Glycoprotein (ABCB1) Function on the Brain Kinetics of Metoclopramide. *J. Nucl. Med.* **2016**, *57*, 309−314.
(28) Wanek, T.; Römermann, K.; Mairinger, S.; Stanek, J.; Sauberer, M.; Filip, T.; Traxl, A.; Kuntner, C.; Pahnke, J.; Bauer, F.; Erker, T.; Löscher, W.; Müller, M.; Langer, O. Factors Governing P-Glycoprotein-Mediated Drug-Drug Interactions at the Blood-Brain Barrier Measured with Positron Emission Tomography. *Mol. Pharm.* **2015**, *12*, 3214−3225.
(29) Bauer, M.; Karch, R.; Neumann, F.; Wagner, C. C.; Kletter, K.; Müller, M.; Löscher, W.; Zeitlinger, M.; Langer, O. Assessment of Regional Differences in Tariquidar-Induced P-Glycoprotein Modulation at the Human Blood-Brain Barrier. *J. Cereb. Blood Flow Metab.* **2010**, *30*, 510−515.
(30) Bauer, M.; Karch, R.; Zeitlinger, M.; Liu, J.; Koepp, M. J.; Asselin, M.-C.; Sisodiya, S. M.; Hainfellner, J. A.; Wadsak, W.; Mitterhauser, M.; Müller, M.; Pataraia, E.; Langer, O. In Vivo P-Glycoprotein Function before and after Epilepsy Surgery. *Neurology* **2014**, *83*, 1326−1331.
(31) Auvity, S.; Caillé, F.; Marie, S.; Wimberley, C.; Bauer, M.; Langer, O.; Buvat, I.; Goutal, S.; Tournier, N. P-Glycoprotein (ABCB1) Inhibits the Influx and Increases the Efflux of 11 C-Metoclopramide across the Blood-Brain Barrier: A PET Study on Non-Human Primates. *J. Nucl. Med.* **2018**, *59*, 1609−1615.
(32) Lee, Y.-J.; Maeda, J.; Kusuhara, H.; Okauchi, T.; Inaji, M.; Nagai, Y.; Obayashi, S.; Nakao, R.; Suzuki, K.; Sugiyama, Y.; Suhara, T. In Vivo Evaluation of P-Glycoprotein Function at the Blood-Brain Barrier in Nonhuman Primates Using [11C]Verapamil. *J. Pharmacol. Exp. Ther.* **2005**, *316*, 647−653.
(33) Schou, M.; Varnäs, K.; Lundquist, S.; Nakao, R.; Amini, N.; Takano, A.; Finnema, S. J.; Halldin, C.; Farde, L. Large Variation in Brain Exposure of Reference CNS Drugs: A PET Study in Nonhuman Primates. *Int. J. Neuropsychopharmacol.* **2015**, *18*, pyv036.
(34) Ke, A. B.; Eyal, S.; Chung, F. S.; Link, J. M.; Mankoff, D. A.; Muzi, M.; Unadkat, J. D. Modeling Cyclosporine A Inhibition of the Distribution of a P-Glycoprotein PET Ligand, 11C-Verapamil, into the Maternal Brain and Fetal Liver of the Pregnant Nonhuman Primate: Impact of Tissue Blood Flow and Site of Inhibition. *J. Nucl. Med.* **2013**, *54*, 437−446.
(35) Takashima, T.; Yokoyama, C.; Mizuma, H.; Yamanaka, H.; Wada, Y.; Onoe, K.; Nagata, H.; Tazawa, S.; Doi, H.; Takahashi, K.; Morita, M.; Kanai, M.; Shibasaki, M.; Kusuhara, H.; Sugiyama, Y.; Onoe, H.; Watanabe, Y. Developmental Changes in P-Glycoprotein Function in the Blood-Brain Barrier of Nonhuman Primates: PET Study with R-11C-Verapamil and 11C-Oseltamivir. *J. Nucl. Med.* **2011**, *52*, 950−957.
(36) Müllauer, J.; Karch, R.; Bankstahl, J. P.; Bankstahl, M.; Stanek, J.; Wanek, T.; Mairinger, S.; Müller, M.; Löscher, W.; Langer, O.; Kuntner, C. Assessment of Cerebral P-Glycoprotein Expression and Function with PET by Combined [11C]Inhibitor and [11C]Substrate Scans in Rats. *Nucl. Med. Biol.* **2013**, *40*, 755−763.
(37) García-Varela, L.; Arif, W. M.; Vállez García, D.; Kakiuchi, T.; Ohba, H.; Harada, N.; Tago, T.; Elsinga, P. H.; Tsukada, H.; Colabufo, N. A.; Dierckx, R. A. J. O.; van Waarde, A.; Toyohara, J.; Boellaard, R.; Luurtsema, G. Pharmacokinetic Modeling of [^{18}F]MC225 for Quantification of the P-Glycoprotein Function at the Blood−Brain Barrier in Non-Human Primates with PET. *Mol. Pharm.* **2020**, *17*, 3477−3486.
(38) Tsukada, H.; Ohba, H.; Kanazawa, M.; Kakiuchi, T.; Harada, N. Evaluation of 18F-BCPP-EF for Mitochondrial Complex 1 Imaging in the Brain of Conscious Monkeys Using PET. *Eur. J. Nucl. Med. Mol. Imaging* **2014**, *41*, 755−763.
(39) Gunn, R. N.; Summerfield, S. G.; Salinas, C. A.; Read, K. D.; Guo, Q.; Searle, G. E.; Parker, C. A.; Jeffrey, P.; Laruelle, M. Combining PET Biodistribution and Equilibrium Dialysis Assays to Assess the Free Brain Concentration and BBB Transport of CNS Drugs. *J. Cereb. Blood Flow Metab.* **2012**, *32*, 874−883.
(40) Fan, J.; de Lannoy, I. A. M. Pharmacokinetics. *Biochem. Pharmacol.* **2014**, *87*, 93−120.
(41) Frey, S.; Pandya, D. N.; Chakravarty, M. M.; Bailey, L.; Petrides, M.; Collins, D. L. An MRI Based Average Macaque Monkey Stereotaxic Atlas and Space (MNI Monkey Space). *Neuroimage* **2011**, *55*, 1435−1442.
(42) Calabrese, E.; Badea, A.; Coe, C. L.; Lubach, G. R.; Shi, Y.; Styner, M. A.; Johnson, G. A. A Diffusion Tensor MRI Atlas of the Postmortem Rhesus Macaque Brain. *Neuroimage* **2015**, *117*, 408−416.
(43) McLaren, D. G.; Kosmatka, K. J.; Oakes, T. R.; Kroenke, C. D.; Kohama, S. G.; Matochik, J. A.; Ingram, D. K.; Johnson, S. C. A Population-Average MRI-Based Atlas Collection of the Rhesus Macaque. *Neuroimage* **2009**, *45*, 52−59.
(44) Ashburner, J. Fast Diffeomorphic Image Registration Algorithm. *Neuroimage* **2007**, *38*, 95−113.
(45) Andersen, P. K. 1. Generalized Estimating Equations. James W. Hardin and Joseph M. Hilbe, Chapman and Hall/CRC, Boca Raton, 2003. No. of Pages: Xiii+ 222 Pp. Price:$79.95. ISBN 1-58488-307-3. *Stat. Med.* **2004**, *23*, 2479−2480.
(46) Liang, K.-Y.; Zeger, S. L. Longitudinal Data Analysis Using Generalized Linear Models. *Biometrika* **1986**, *73*, 13−22.
(47) Ma, Y.; Mazumdar, M.; Memtsoudis, S. G. Beyond Repeated-Measures Analysis of Variance. *Reg. Anesth. Pain Med.* **2012**, *37*, 99−105.
(48) Ikoma, Y.; Takano, A.; Ito, H.; Kusuhara, H.; Sugiyama, Y.; Arakawa, R.; Fukumura, T.; Nakao, R.; Suzuki, K.; Suhara, T. Quantitative Analysis of 11C-Verapamil Transfer at the Human Blood-Brain Barrier for Evaluation of P-Glycoprotein Function. *J. Nucl. Med.* **2006**, *47*, 1531−1537.
(49) Muzi, M.; Mankoff, D. A.; Link, J. M.; Shoner, S.; Collier, A. C.; Sasongko, L.; Unadkat, J. D. Imaging of Cyclosporine Inhibition of P-Glycoprotein Activity Using 11C-Verapamil in the Brain: Studies of Healthy Humans. *J. Nucl. Med.* **2009**, *50*, 1267−1275.
(50) Kuntner, C.; Bankstahl, J. P.; Bankstahl, M.; Stanek, J.; Wanek, T.; Stundner, G.; Karch, R.; Brauner, R.; Meier, M.; Ding, X.; Müller, M.; Löscher, W.; Langer, O. Dose-Response Assessment of Tariquidar and Elacridar and Regional Quantification of P-Glycoprotein Inhibition at the Rat Blood-Brain Barrier Using (R)-[11C]Verapamil PET. *Eur. J. Nucl. Med. Mol. Imaging* **2010**, *37*, 942−953.
(51) Verbeek, J.; Syvänen, S.; Schuit, R. C.; Eriksson, J.; de Lange, E. C.; Windhorst, A. D.; Luurtsema, G.; Lammertsma, A. A. Synthesis and Preclinical Evaluation of [11C]D617, a Metabolite of (R)-[11C]Verapamil. *Nucl. Med. Biol.* **2012**, *39*, 530−539.
(52) Syvänen, S.; Lindhe, Ö.; Palner, M.; Kornum, B. R.; Rahman, O.; LÅngström, B.; Knudsen, G. M.; Hammarlund-Udenaes, M. Species Differences in Blood-Brain Barrier Transport of Three Positron Emission Tomography Radioligands with Emphasis on P-Glycoprotein Transport. *Drug Metab. Dispos.* **2009**, *37*, 635−643.
(53) Katoh, M.; Suzuyama, N.; Takeuchi, T.; Yoshitomi, S.; Asahi, S.; Yokoi, T. Kinetic Analyses for Species Differences in P-Glycoprotein-Mediated Drug Transport. *J. Pharm. Sci.* **2006**, *95*, 2673−2683.
(54) Damont, A.; Goutal, S.; Auvity, S.; Valette, H.; Kuhnast, B.; Saba, W.; Tournier, N. Imaging the Impact of Cyclosporin A and Dipyridamole on P-Glycoprotein (ABCB1) Function at the Blood-Brain Barrier: A [11C]-N-Desmethyl-Loperamide PET Study in Nonhuman Primates. *Eur. J. Pharm. Sci.* **2016**, *91*, 98−104.
(55) Luurtsema, G.; Molthoff, C. F. M.; Schuit, R. C.; Windhorst, A. D.; Lammertsma, A. A.; Franssen, E. J. F. Evaluation of (R)-[11C]Verapamil as PET Tracer of P-Glycoprotein Function in the Blood-Brain Barrier: Kinetics and Metabolism in the Rat. *Nucl. Med. Biol.* **2005**, *32*, 87−93.
(56) Onoe, H.; Inoue, O.; Suzuki, K.; Tsukada, H.; Itoh, T.; Mataga, N.; Watanabe, Y. Ketamine Increases the Striatal N-[11C]-Methylspiperone Binding in Vivo: Positron Emission Tomography Study Using Conscious Rhesus Monkey. *Brain Res.* **1994**, *663*, 191−198.
(57) Mohs, R. C.; Greig, N. H. Drug Discovery and Development: Role of Basic Biological Research. *Alzheimer's Dementia* **2017**, *3*, 651−657.

https://dx.doi.org/10.1021/acs.molpharmaceut.0c01014
Mol. Pharmaceutics XXXX, XXX, XXX−XXX